J. Materials, Conc. Struct. Pavements, JSCE, No. 704/V-55, 257-270, 2002 May

NUMERICAL ANALYSIS ON INTERFACIAL FRACTURE MECHANISM OF EXTERNALLY FRP-STRENGTHENED STRUCTURAL MEMBERS

Zhishen WU [1] and Jun YIN [2]

[1]Member of JSCE, Dr. of Eng., Associate Professor, Dept. of Urban & Civil Eng., Ibaraki University
(Nakanarusawa-cho 4-12-1, Hitachi Ibaraki 316-8511, Japan)
[2]Student Member of JSCE, MS of Eng. Dept. of Urban & Civil Eng., Ibaraki University
(Nakanarusawa-cho 4-12-1, Hitachi Ibaraki 316-8511, Japan)

Debonding along FRP-concrete interface is regarded as one of the most significant fracturing behaviors in FRP-strengthened concrete structures. To model FRP-concrete interfacial bond behavior in experiment, several kinds of local shear stress-relative displacement (τ–δ) relationships are proposed. The results of finite element simulation and theoretical derivation are compared. The linear ascending and descending τ–δ relationship is regarded as an applicable and accurate model, and is used in this paper. The observed experimental failure modes and cracking behaviors are simulated through a parametric study of bond interface properties and concrete fracture energy, whose effects on load-carrying capacity and concrete crack distribution are studied.

Key Words: *FRP-strengthening effect, bond interface, debonding propagation, interfacial fracture energy, crack distribution*

1. INTRODUCTION

The application of fiber reinforced polymer (FRP) sheets, as an externally bonded reinforcement, is generally accepted as an effective technique of strengthening and upgrading structurally inadequate or damaged concrete structures. FRP sheets offer unique advantages, such as high strength-to-weight ratio and considerably good resistance to corrosion, over the conventional steel bars and plates that cannot provide satisfactory service life. In addition, the flexibility of FRP sheets makes it to be easily bonded to any shape of surface.

Although the FRP strengthening effects are considered remarkable in practice, the mechanical behavior of FRP reinforcement, especially along the FRP-concrete bond interface, is not fully understood. Some of new fracture phenomena in FRP-strengthened structures such as debonding of FRP sheets, crack localization and distribution in concrete cannot yet be explained properly. In order to have a good understanding of FRP strengthening effect in concrete structures, recently much work has been done through theoretical analysis[1),2),3),4),5)], as well as the experimental approaches[6),7),8),9)].

The important mechanical behavior of FRP-strengthened concrete members is the stress transfer between FRP sheets and concrete through bond interface. Good interfacial bond provides effective stress transfer between concrete and FRP sheets, thus enhancing the strengthening effect of FRP sheets. Täljsten[1)] theoretically derived the equation that calculates the load carrying capacity of FRP-bonded concrete prism. The maximum load could be expressed as a function of interfacial fracture energy, Young's modulus and thickness of FRP composites. More investigations of the stress transfer in FRP-concrete bond interface were done by Yuan et al.[2)] and Nishida et al.[5)], in which several types of nonlinear shear stress versus relative displacement τ–δ relationships were proposed and the corresponding shear stress distributions along the bond interface were described. Wu and Niu[3),4)] developed a methodology for predicting the debonding failure load and the interaction between concrete flexural crack and interfacial shear stress of RC beams

based on linear elastic beam theory. In the experimental aspects, Chajes et al.[6] studied the bond strength and force transfer of composite adhered to concrete by a single-lap shear test. The similar experiments were carried out by Yoshizawa et al.[7] and Wu et al.[8], through which the interfacial mode II fracture energy was identified and the τ–δ_t relationship was predicted indirectly by several approaches such as using the measured FRP strain distribution along the bond interface. Moreover, a series of tests on FRP-strengthened concrete beams were performed by Wu et al.[9]. The structural responses with different concrete compression strength, interfacial bond condition and amount of FRP sheets were summarized. Different kinds of failure modes such as interfacial debonding and FRP sheet rupture were recorded.

In this paper, the FRP-concrete interfacial bond behavior is further studied by finite element simulation. Based on the numerical analysis of interfacial crack propagation by Yin et al.[10), 11)], a general τ–δ_t model is presented, which considers the elastic-inelastic continuous deformation and discontinuous crack. In shear bond test, several τ–δ_t relationships are used in the finite element simulation. Compared with the experimental results by Yoshizawa[8] and Wu et al.[9], it is found that a linear ascending-descending τ–δ_t relationship can essentially reflect the debonding behavior in experiments. Such a τ–δ_t relationship is adopted in numerical simulation of FRP-strengthened concrete beams in three point bending tested by Wu et al.[10]. A parametric study that considers the effects of the properties of bond interface and concrete fracture energy is carried. Although the investigation of RC beams has more practical meanings, what is focused in this study is to make a basic understanding on FRP strengthening effect when interfacial fracture happens along FRP-concrete interface. Therefore, a plain concrete beam strengthened with FRP sheets is chosen as the research subject. On the other hand, this research is considered to be useful for discussing FRP strengthening effect in FRP-strengthened plain concrete structures, such as concrete tunnel linings.

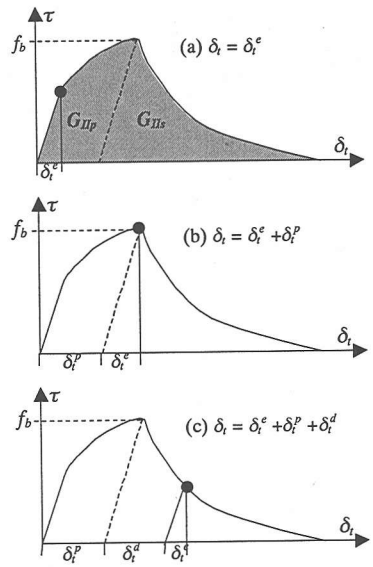

Fig.1 A general τ–δ_t relationship

2. INTERFACE DEBONDING MODEL

Debonding along FRP-concrete bond interface is a most significant fracturing behavior in FRP-strengthened concrete structures, which can be assumed as mode II fracture since the shear stress is much more dominant than the normal stress in bond interface. To describe the interfacial debonding, it is necessary to introduce a proper constitutive model for interfacial bond mechanical behavior. It could be expressed as a relationship of local shear stress, τ, versus relative shear displacement, δ_t, between FRP sheets and concrete matrix, as shown in **Fig.1**, where f_b is the local bond strength. In general, the relative shear displacement, δ_t, can be divided into an elastic part δ_t^e, a plastic part δ_t^p and a discontinuous part δ_t^d, yielding the following equation,

$$\delta_t = \delta_t^e + \delta_t^p + \delta_t^d \qquad (1)$$

The area under the τ–δ_t curve, as shown in **Fig.1**(a), denotes the total fracture energy, G_{IIb}, which is defined as the energy required to bring a unit bond surface to complete fracture. Generally, the total fracture energy, G_{IIb}, consists of the irreversible work, G_{IIp}, for the plastic deformation in continuum stage, and the softening fracture

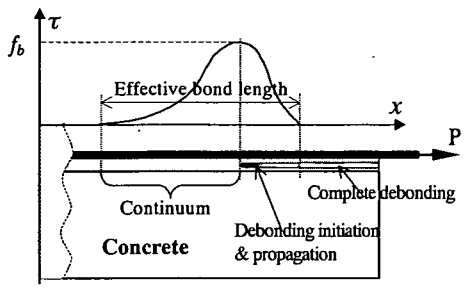

Fig.2 Shear stress distribution along bond interface

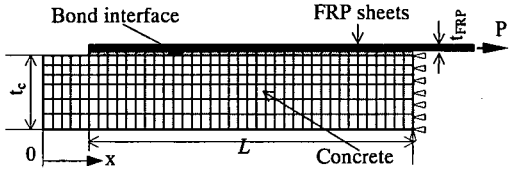

Fig.3 Shear bond test of FRP-bonded concrete

energy, G_{IIs}, consumed to create complete debonding after discontinuity occurs.

$$G_{IIb} = G_{IIp} + G_{IIs} \quad (2)$$

The shear stress distribution along the FRP-concrete bond interface can be schematically shown in **Fig.2**. The bond interface is continuous during elastic and plastic (if considered) loading before bond strength is reached. Thereafter, debonding (discontinuity) initiates and starts to propagate with the decrease of shear stress until complete vanishing of the shear stress. The bond length, providing the force transfer between FRP and concrete, is defined as effective bond length that may be affected by the shape of τ–δ_l curves.

3. SHEAR BOND TEST

A concrete prism strengthened with FRP sheets is simulated for discussing the shear bond behavior. The experimental procedure can be referred to Yoshizawa's[8] work. The schematic sketch and is presented in **Fig.3**, where L is the bond length of FRP sheets, b_c=b_{FRP}=40mm is the width of bonded FRP sheets and concrete prism, t_c = 60mm, and t_{FRP} = 0.22mm are the thickness of concrete prism and FRP sheets, respectively.

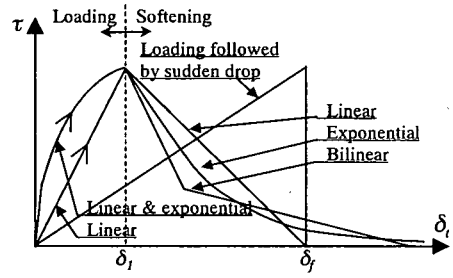

Fig.4 Several proposed relationships

As stated previously, the τ–δ_l relationship can be modeled in various forms. Most of them are composed of the loading stage with increasing stress and the subsequent softening stage where the shear stress decreases gradually to zero, except one limit case in which there is only the elastic loading followed by a sudden drop of shear stress, as presented in **Fig.4**. The objective of this section is to simulate the interfacial bond behavior, to compare the FE results with experimental data by Yoshizawa et al.[8] and theoretical solutions derived by Yuan et al.[3], and finally to find an appropriate interfacial τ–δ_l relationship.

Firstly, the effect of different τ–δ_l relationships on the shear stress distribution is analyzed. Six types of τ–δ_l relationships, listed in **Table 1** and shown in **Fig.5**, are investigated. The other material properties are defined as follows: Young's modulus of concrete E_c=3.2×10^{4}MPa, Poisson ratio ν=0.15, total interfacial fracture energy G_{IIb}=1.2N/mm, bond strength τ_{max}=8.0MPa, E_{FRP}=2.3×10^{5}MPa. Except the limit case of SB6, the other τ–δ_l relationships follow an assumption that the area under τ–δ_l curves before maximum bond strength is set 1/6 of the total fracture energy G_{IIb}. The stiffness of linear part in case SB4 and SB5 is set 5 times of that in case SB1 through SB3. And the linear part terminates when the shear stress reaches 1/10 of bond strength.

According to the discussion of fracture energy dissipation in the previous section, the total fracture energy G_{IIb} is considered separately as the sum of G_{IIp} and G_{IIs} in case of SB4 and SB5 with a linear-exponential loading curve. But in the cases through SB1 to SB3, it is assumed that all the fracture energy G_{IIb} is completely consumed by formation of discontinuous crack with little plastic

Table 1 Different types of τ–δ_t relationships

Case	Loading	Softening
SB1	Linear	Exponential
SB2	Linear	Bilinear
SB3	Linear	Linear
SB4	Linear-exponential	Exponential
SB5	Linear-exponential	Linear
SB6	Linear	—

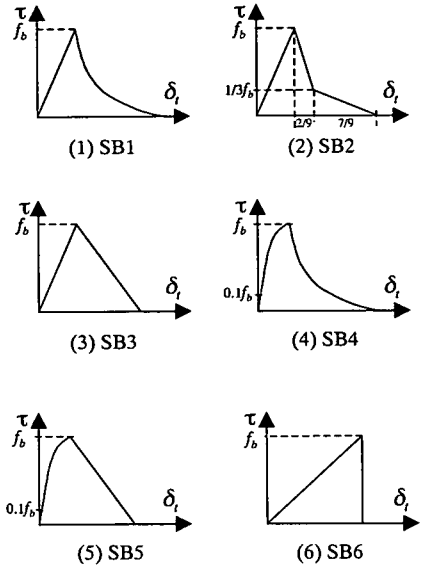

Fig.5 Six types of τ–δ_t relationships

deformation, so that only linear curve is used before bond strength is reached.

In the finite element simulation, concrete prism is discretized by 4-node plane stress elements. Near the bond interface, three layers of 8×8mm plane stress elements are used. For the rest of concrete, coarse mesh by 8×12mm plane stress element is adopted. If a crack happens in concrete, it is simulated by the rotating smeared crack model. The FRP sheets and bond interface are discretized by truss element and line-to-line interface element[12], respectively, in which FRP sheet is linear elastic until rupture, whereas debonding behavior of bond interface is modeled by the proposed τ–δ_t relationships.

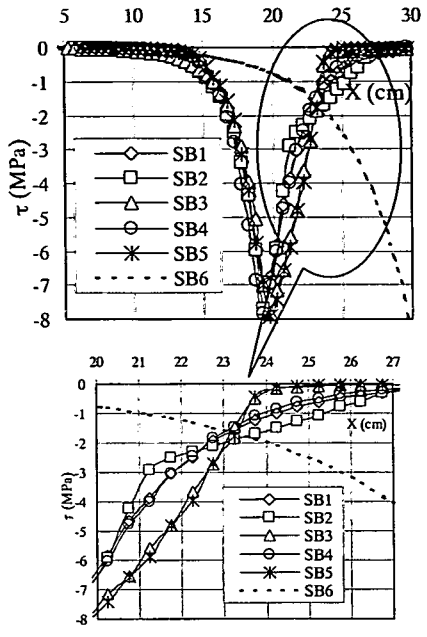

Fig.6 Shear stress distribution along bond interface

The shear stress distributions, based on the different τ–δ_t relationships, along the bond interface are shown in **Fig.6**. Before shear stress reaches the bond strength, the results of cases through SB1 to SB5 do not present big difference. But in the softening stage, the difference can be seen. Cases of SB3 and SB5 with linear softening curve have a quick decrease of shear stress, while the cases with bilinear and exponential softening curves have quick shear stress degradation firstly, followed by a gradual decreasing to zero.

In addition, theoretical solutions of two typical models, model I and model II, derived by Yuan et al.[2], according to the τ–δ_t relationships of SB6 and SB3 following the Eq.(3) and Eq.(4) respectively, are compared to the finite element results in **Fig.7**, with the assumption that bending effect is neglected.

For model I according to case SB6,

$$\tau = \tau_{max} \frac{\cosh(\lambda x)}{\cosh(\lambda L)} \tag{3.a}$$

where

$$\lambda = \sqrt{\frac{\tau_{max}^2}{2G_{II}} \left(\frac{1}{E_{FRP} t_{FRP}} + \frac{b_{FRP}}{b_c E_c t_c} \right)} \tag{3.b}$$

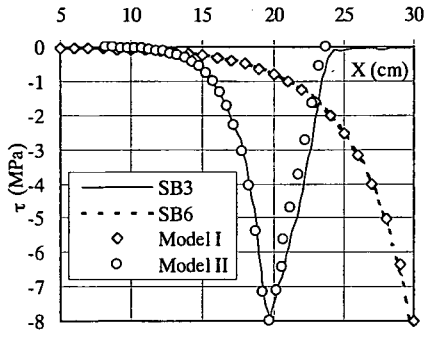

Fig.7 Comparison with theoretical results

and for model II,

$$\tau = \tau_{max} \frac{\cosh(\lambda x)}{\cosh[\lambda(L-a)]} \quad (0<\delta_t<\delta_1) \qquad (4.a)$$

$$\tau = -\tau_{max} \left\{ \begin{array}{l} \frac{\lambda_1}{\lambda_2} \tanh[\lambda_1(L-a)] \sin[\lambda_2(x-L+a)] \\ +\cos[\lambda_2(x-L+a)] \end{array} \right\} \quad (\delta_1<\delta_t<\delta_f) \qquad (4.b)$$

where

$$\lambda_1 = \sqrt{\frac{\tau_{max}}{\delta_1}\left(\frac{1}{E_{FRP}t_{FRP}} + \frac{b_{FRP}}{b_c E_c t_c}\right)} \qquad (4.c)$$

$$\lambda_2 = \sqrt{\frac{\tau_{max}}{\delta_f - \delta_1}\left(\frac{1}{E_{FRP}t_{FRP}} + \frac{b_{FRP}}{b_c E_c t_c}\right)} \qquad (4.d)$$

$$a = \frac{1}{\lambda_2} \arctan\left(\frac{\lambda_1}{\lambda_2}\right) \qquad (4.e)$$

L is the bond length of FRP sheets. From **Fig.7**, the finite element results accurately match the theoretical solutions.

Fig.8 shows the relationship between the load and the pull out displacement. At the beginning of the loading process, the load displacement curves through SB1 to SB5 are almost the same and match the experimental results. The difference takes place only when the load tends to approach the maximum load. The model with linear softening curve increases to P_{max} quickly, while the models with bilinear and exponential softening curves gradually reach P_{max}. It is found that the value of P_{max} in

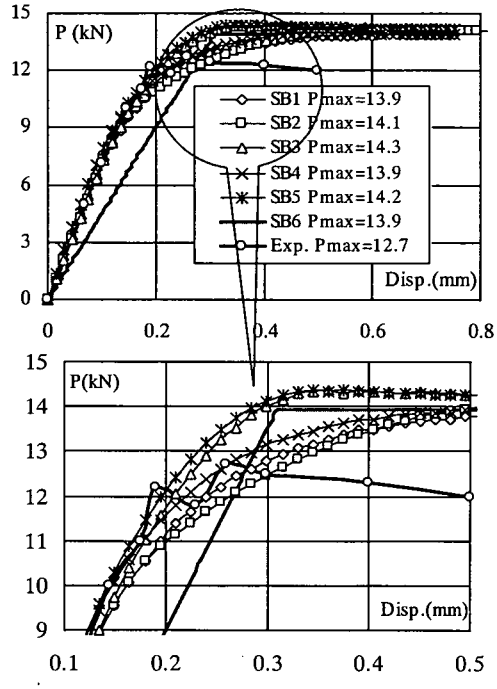

Fig.8 Load displacement curves

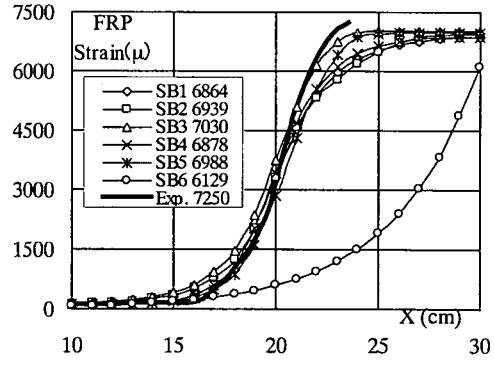

Fig.9 FRP strain distribution

experiments is less than that of FE results. This may be caused by the instability near the stage of complete debonding in experiments.

Moreover, **Fig.9** shows the FE results of strain distribution in FRP sheets. The experimental result is actually obtained at the right load end. To make a good comparison with the simulation results, the experimental curve is shifted to the left as adjustment. Compared to the experimental one, it is found that the linear softening curve agrees better

than other softening curves do. Also, considering the FE results that during loading stage the linear curve and linear-exponential curve do not cause obvious difference, the simple linear one is naturally chosen. Consequently, a τ–δ_l relationship with linear ascending-descending curve, as presented in SB3, is considered to be an applicable model to capture interfacial debonding behavior with enough accuracy. Following the assumption that the area under τ–δ_l relationships before maximum bond strength is set 1/6 of the total fracture energy G_{IIb}, the initial bond interface stiffness is about equal to $K_b=f_b/\delta_1= 1.6\times10^2$N/mm^3. Although the value of initial bond interface stiffness, to some extent, depends on the bonding quality of FRP sheets and the properties of concrete surface, it could be considered as a reference parameter.

In a whole viewpoint of bond behavior, choosing different τ–δ_l relationships, including the limit case of SB6, do not affect the ultimate load P_{max} and maximum strain ε_{max} in FRP sheets. It can be explained that the total interfacial fracture energy is an important parameter to determine the stress transfer ability of FRP-concrete bond interface and, the ultimate load P_{max}. This conclusion has been also obtained through the theoretical solution[1), 2)], as written

$$P_{max}=b_{FRP}\sqrt{\frac{2G_{II}}{\frac{1}{E_{FRP}t_{FRP}}+\frac{b_{FRP}}{b_cE_ct_c}}} \quad (5)$$

$$\varepsilon_{max}=\frac{P_{max}}{E_{FRP}t_{FRP}b_{FRP}} \quad (6)$$

Calculated by Eq.(5) and Eq.(6), the theoretical values of ultimate load and maximum strain of FRP sheets are P_{max} = 13.87kN, ε_{max} = 6851μ, respectively. An error comparison is shown in **Table 2**, in which most of errors are within 3%, except the limit case SB6 that may be due to the sudden loss of shear stress when the shear stress of first integral point reaches to τ_{max}. This usually causes the numerical instability in FE simulation.

From Eq.(5), it is found that the ultimate load P_{max} is not only a function of G_{IIb}, but also depends on the E_{FRP} and t_{FRP}. The FE simulation results

Table 2 Comparison of FE and theoretical results

	P_{max}(kN)	Error	ε_{max}(μ)	Error
Theory	13.87	----	6851	----
SB1	13.9	0.22%	6864	0.19%
SB2	14.1	1.66%	6939	1.28%
SB3	14.3	3.10%	7030	2.61%
SB4	13.9	0.22%	6878	0.39%
SB5	14.2	2.38%	6988	2.0%
SB6	13.9	0.22%	6129	10.5%

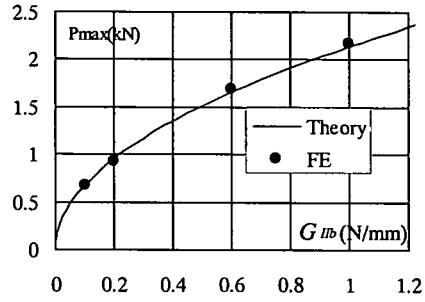

Fig.10 Relation between P_{max} and G_{IIb}

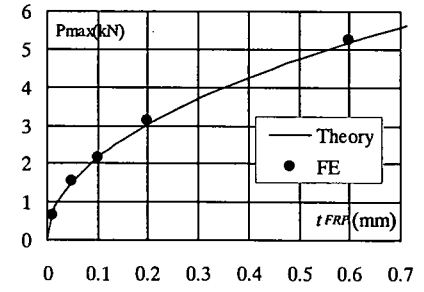

Fig.11 Relation between P_{max} and t_{FRP}

match well the theoretical solution. The relations between the ultimate load P_{max}, interfacial fracture energy G_{IIb} and thickness of FRP sheets t_{FRP} are figured out in **Fig.10** and **Fig.11**. The constant properties are $E_c=3.2\times10^4$MPa, $b_c=b_{FRP}=10$mm, $t_c=60$mm, $E_{FRP}=2.3\times10^5$MPa. In **Fig.10**, the maximum loads in four cases with G_{IIb} =0.1, 0.2, 0.6 and 1.0N/mm are compared to the theoretical results, in which the thickness of FRP sheet is chosen t_{FRP}=0.1mm. **Fig.11** shows five finite element simulation results of t_{FRP}=0.01, 0.05, 0.1, 0.2 and 0.6mm with the same G_{IIb}=1.0N/mm. It can be seen that the FE results approximately match the theoretical ones.

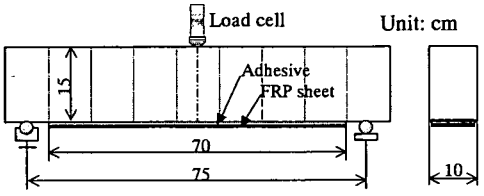

Fig.12 Dimension of tested specimens

4. FRP-STRENGTHENED CONCRETE BEAMS

In this section, the FE analysis is carried out, based on an experimental program of FRP-strengthened concrete beams under 3-point bending by Wu et al.[9], as shown in **Fig.12**. The different kinds of observed failure modes in the experiments are simulated. The factors of properties of bond interface and concrete that affect the cracking behavior in concrete are also discussed in detail.

(1) Review of Experimental Observations

From the experimental observation, there are two typical failure modes, i.e., the interfacial debonding of FRP sheets from the bond interface and the rupture of FRP sheets. In the tested beams that failed in interfacial debonding, there are also three types of debonding forms. The first type happens in adhesive layer due to weak bond condition and initiates from the root of mid span. The second one takes place in concrete with formation of micro-cracks along the bond interface. Debonding also starts to propagate from mid span. The corresponding crack patterns of concrete are presented in **Fig. 13**(a) and **Fig. 13**(b), respectively. A common point of these two types of debonding failures is that only one dominant flexural crack locally occurs and develops at mid span. The third type of debonding initiates from the root of a diagonal crack that has formed near the first flexural crack at mid span. Then, it follows micro-crack development along the bond interface, as shown in **Fig. 13**(c).

On the other hand, for the beams of FRP rupture failure, there are also two representative cracking behaviors: 1) one dominant flexural crack at mid-span with several surrounding diagonal micro-cracks as shown in **Fig. 13**(d), and 2) multiple flexural cracks are distributed around the mid-span, as shown in **Fig. 13**(e). The load

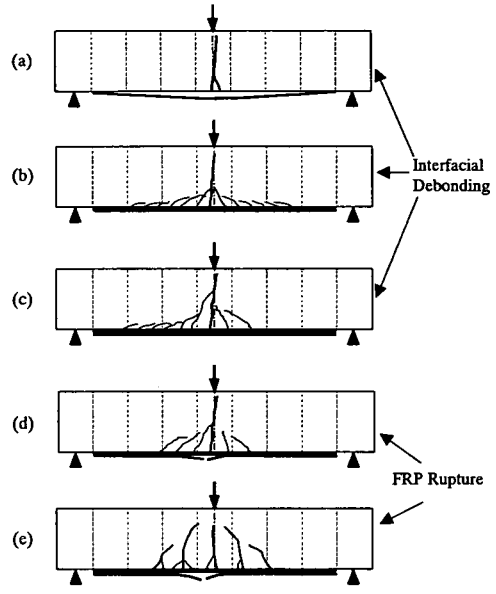

Fig. 13 Failure modes and crack patterns

capacity of the beams that failure in FRP rupture is universally higher than that of beams in debonding failure.

(2) Material Properties in Numerical Simulation

In the FE analysis, the material properties of concrete beams are Young's modulus of concrete E_c=2.5×10^{4}MPa, Poisson ratio ν =0.15, tensile strength of concrete $f_t = 0.23 f_c^{2/3}$ =3.31MPa, in which f_c=53.9MPa is the concrete compressive strength referred to the test data. The concrete fracture energy G_{Ic} is thought of an unknown material property. The Young's modulus of FRP sheet is E_{FRP}=2.3×10^{5}MPa, rupture stress of FRP sheet is σ_r=3.35×10^{3}MPa, which are according to the specification of FRP sheets provided by the manufacturer. A simple linear ascending-descending τ–δ_t relationship, as used in the case of SB3 in shear bond test, is adopted in the following finite element simulations. Because of the lacking information of the properties in bond interface, stiffness of bond interface K_b, bond strength f_b and interfacial fracture energy G_{IIb} are also considered as unknowns.

Due to the symmetry of load condition and dimension of the structure, half of the FRP-strengthened beam is discretized by 10×10mm

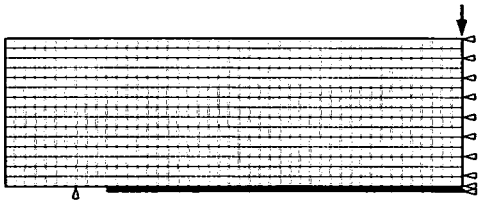

Fig.14 Mesh discretization and boundary condition

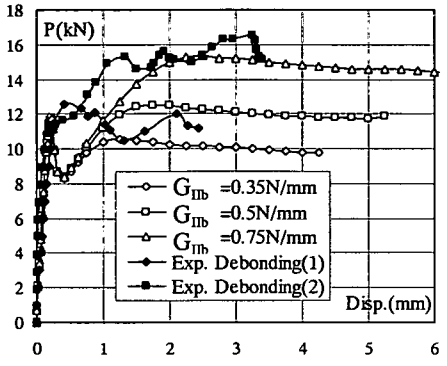

Fig.15 Load-displacement curves with different G_{IIb}

plane stress element with proper boundary conditions, as shown in **Fig.14**. A parametric study of FE simulation is carried out in 4 categories, concrete fracture energy, bond strength, interfacial fracture energy and stiffness of bond interface, to separately discuss their effects on the load carrying capacity, deformational and fracturing behaviors of FRP-strengthened beam.

(3) Interfacial Fracture Energy G_{IIb}

Known from the previous study in shear bond case[1), 2), 10)], the interfacial fracture energy G_{IIb} is a key parameter to describe the stress transfer capacity of bond interface. As shown in Eq.(5), maximum load P_{max} is uniquely determined by G_{IIb} with constant E_{FRP} and t_{FRP}. How G_{IIb} affects the behavior of FRP-strengthened concrete beams is studied as follows.

With the same concrete fracture energy G_{Ic}=0.25N/mm, bond strength f_b=1.8MPa and interfacial bond stiffness K_b=160.0N/mm^3, the interfacial fracture energy is varied, G_{IIb}=0.35, 0.5 and 0.75N/mm. The simulation results of load-displacement curve and crack patterns are compared in **Fig.15** and **Fig.16** respectively.

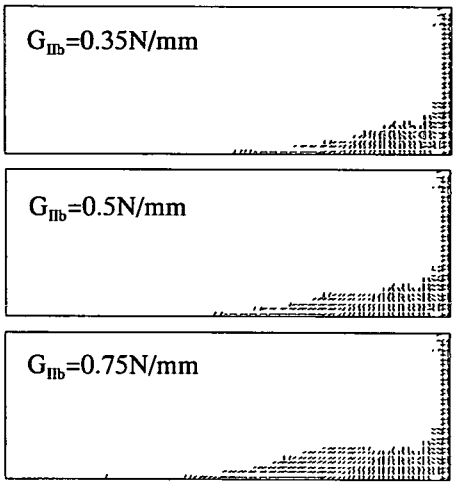

Fig.16 Crack patterns with different G_{IIb}

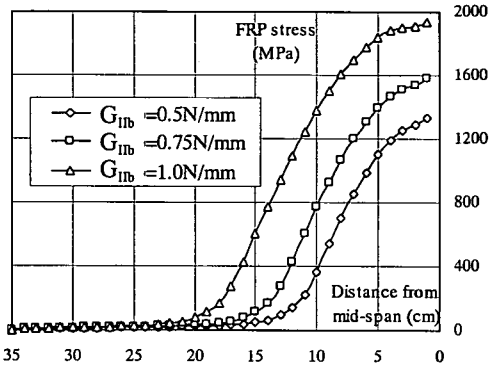

Fig.17 Stress distribution of FRP sheets

All three beams are subjected to debonding failure because the bond strength f_b=1.8MPa is rather low. As shown in **Fig.16**, there are no more dominant flexural cracks in concrete except the one at mid span. With increase of interfacial fracture energy G_{IIb}, the scope of cracked concrete along bond interface becomes longer. This may be explained that higher G_{IIb} provides longer effective bond length between FRP sheets and concrete, as shown in **Fig.17**. The debonding in case of G_{IIb}=0.35N/mm represents the type shown in **Fig.13**(a), while the cases of G_{IIb}=0.5 and 0.75N/mm are similar to the debonding type as shown in **Fig.13**(b). In addition, the load carrying capacity is also enhanced with increase of G_{IIb} and finally approaches to constants in each case after

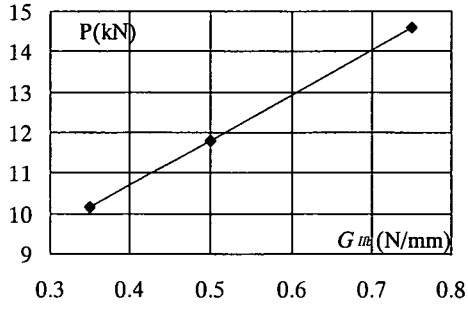

Fig.18 Relation between P and G_{IIb}

the occurring of interfacial debonding propagation. The stress distribution of FRP sheet shows that the maximum FRP stress also increases with increase of interfacial fracture energy, G_{IIb}. In experiment, the two debonding failure beams that exhibited crack patterns as shown in **Fig.13**(a) and **Fig.13**(b) respectively, show the similar results.

Fig.18 gives a relation between the ultimate load P and interfacial fracture energy G_{IIb}. It exhibits an approximately linear relation between P and G_{IIb}, which holds only if the FRP-strengthened concrete beam fails in interfacial debonding with a single concrete flexural crack at mid-span. For the cases with multiple concrete flexural cracks, the relationship is no longer unique and other factors such as number of flexural cracks and their interval may affect P_{max}.

(4) Local Bond Strength f_b

Interfacial bond strength is defined as the maximum shear stress that the FRP-concrete bond interface can bear. When the shear stress reaches the local bond strength, the interfacial debonding is initiated and local shear stress starts to decrease following the softening branch of τ–δ_l relationship. In experiment, the debonding failure was observed either in adhesive layer or in bonded concrete surface. Herein, the bond strength is considered as the property of adhesive. The debonding in concrete should be related to the material properties of concrete, such as fracture energy. This discussion will be made in later subsection.

To compare the different responses caused by the bond strength, 4 cases, with bond strength f_b=1.0, 1.8, 2.5 and 3.0MPa, are simulated. Other

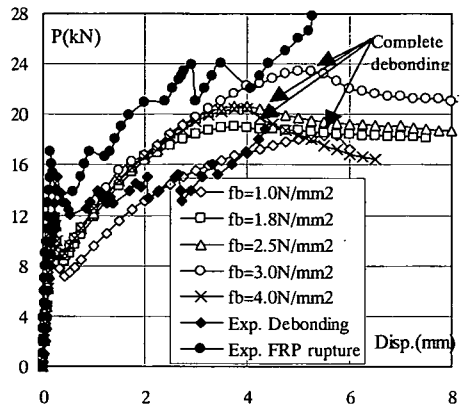

Fig. 19 Load-displacement curves with different f_b

material properties, Concrete fracture energy G_{Ic}=0.25N/mm, interfacial fracture energy G_{IIb}= 1.2N/mm and stiffness of bond interface K_b= 160N/mm^3, are kept unchanged.

As shown in **Fig.19**, the peak load increases with the increasing bond strength. Noticing the τ–δ_l relationship used to model the interfacial debonding, before shear stress in FRP-concrete interface exceeds the bond strength, the higher the shear stress can reach, the more stress can be transferred from FRP sheets to concrete so as to cause more concrete to crack. Since the external load needs to do more works to create the cracks, the peak load increases. In addition, when a complete debonding is formed, the load-carrying capacity would not increase any more and start to follow a loading drop.

Afterwards, the load decreases and approaches to a constant value. The ultimate loads of cases f_b = 10, 18, 25kgf/cm^2 are very close because the interfacial fracture energies are chosen the same value and interfacial debonding mainly happens in the bond layer. The ultimate load of case f_b= 30kgf/cm^2 is higher than the previous three cases. This may be due to much more concrete cracks caused by interfacial stress transfer. Also, interfacial debonding partly occurs in form of concrete crack near the bond interface, as seen in **Fig.21**. Hence, the extra works done to create more cracks in concrete keeps the ultimate load higher

From the comparison of FRP sheets stress distributions where a complete debonding is formed, as shown in **Fig.20**, the maximum stress

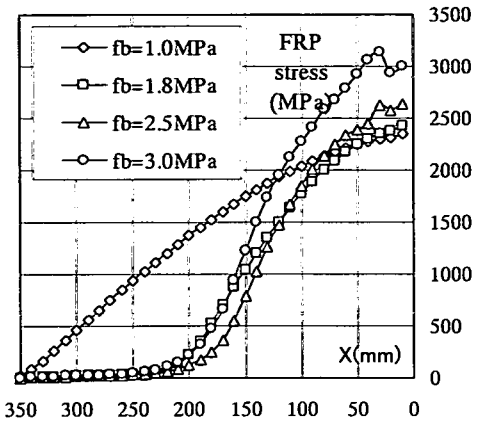

Fig. 20 Stress distribution of FRP sheets

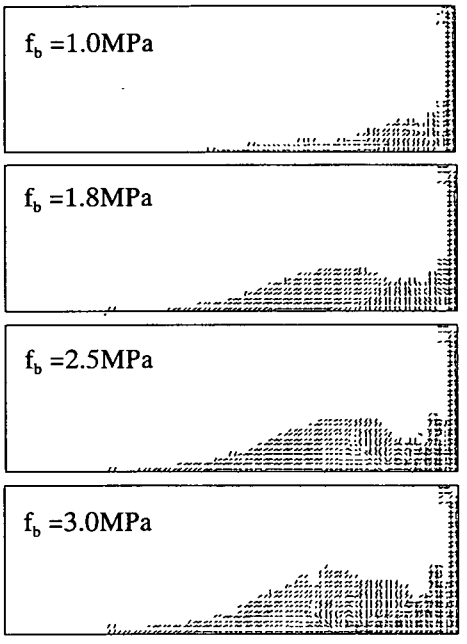

Fig. 21 Crack patterns with different f_b

of case f_b=3.0MPa is about 3200MPa, apparently higher than that of other cases, and is near to the rupture stress of FRP sheets. In the case of f_b=1.0MPa, the effective bond length is longer than the other cases. It is because that the same interfacial fracture energy G_{IIb} is chosen so that the local τ–δ_l relationship follows a more gradual softening curve. Such a behavior is similar to the bond-slip in steel fiber reinforced concrete, in which the friction between cracked concrete and the steel fibers shows plastic behavior.

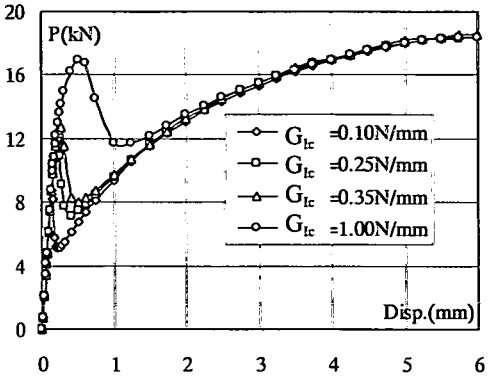

Fig. 22 Load-displacement curves for situation (1)

Compared to the experiments in **Fig.19**, it is found that the beam of high bond strength with f_b = 3.0MPa is similar to the tested beam of FRP rupture, as shown in **Fig.13**(d), while the failure mode in case of low bond strength with f_b =1.0MPa resembles interfacial debonding failure, whose crack pattern is similar to experimental one as shown in **Fig.13**(a).

It is suggested that the bond strength have effects on the peak load. However, the ultimate load capacity mainly depends on the interfacial fracture energy G_{IIb} if interfacial debonding happens.

(5) Concrete Fracture Energy G_{Ic}

Concrete fracture energy is considered as a key material property to describe the brittleness of concrete in crack propagation. Concrete cracks include the flexural, diagonal crack caused by bending and the interfacial crack along the bond interface. It influences significantly the structural response of FRP-strengthened concrete beams.

The effect of concrete fracture energy, with G_{Ic}=0.1, 0.25, 0.35 and 1.0N/mm, is discussed under two types of basic situations: (1) weaker interfacial bond with f_b=1.0MPa and G_{IIb}=1.2N/mm, (2) better interfacial bond with f_b=2.5MPa, G_{IIb}=2.0N/mm. For both situations, the initial stiffness of bond interface is K_b=160.0N/mm^3.

For situation (1), concrete fracture energy only affects the crack propagation at mid span. Because the interfacial bond is considerably weaker, when

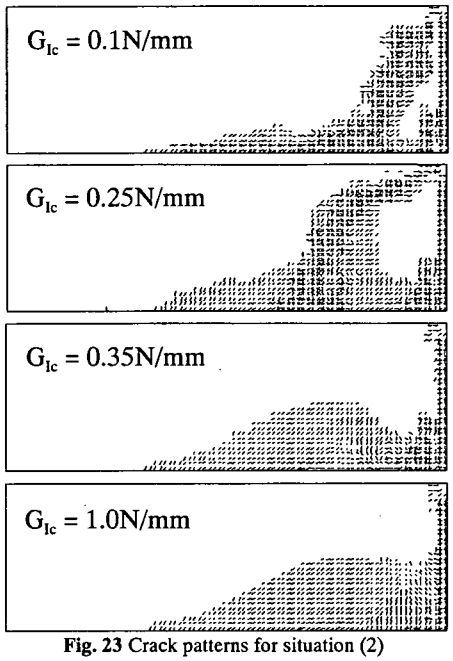

Fig. 23 Crack patterns for situation (2)

interfacial crack is initiated and the complete debonding is formed around the root of crack flexural crack at mid span, it propagates rapidly towards the end of FRP sheets and leads to final debonding failure. Hence, simply increasing concrete fracture energy does not improve FRP strengthening effect if FRP-concrete interface is too weak, as shown in **Fig.22**.

For situation (2), both bond strength f_b and interfacial fracture energy G_{IIb} are increased. From the crack pattern of case G_{Ic}=0.1N/mm, as shown in **Fig.23**, a diagonal crack in concrete occurs near the flexural crack at mid span. Finally, the interfacial debonding propagates in concrete from the root of the diagonal crack along the bond interface. When G_{Ic} is increased to 0.25N/mm, a secondary flexural crack pattern occurs about 13cm away from the first one at mid span. The crack patterns of both cases are similar to the experimental result, as shown in **Fig.13**(c).

In the load-displacement curve of **Fig.24**, there is a second loading drop at deflection of 3.5cm, reflecting local stress release due to localized crack propagation of the second flexural crack. The load level is also enhanced. The maximum stress of FRP sheets reaches the rupture stress, σ_r =3.35×10^{3}MPa, marking the FRP sheets rupture as shown in **Fig.25**.

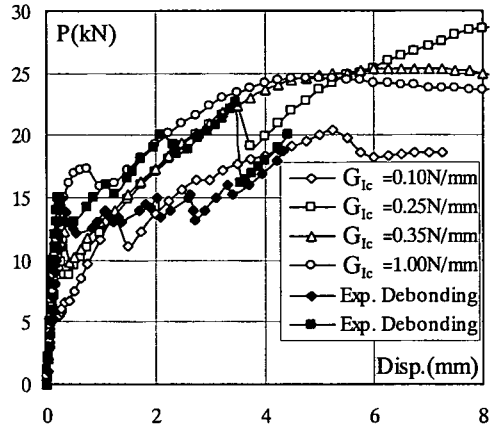

Fig.24 Load-displacement curves for situation (2)

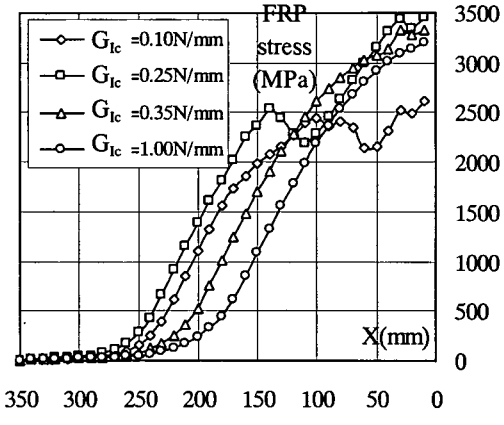

Fig.25 FRP stress distributions for situation (2)

With further increase to G_{Ic}=0.35 and 1.0N/mm, the localized flexural or diagonal cracks disappear. Cracks tend to be distributed, and are considered to be similar to the experimental cases shown in **Fig.13**(d) and **Fig.13**(e), respectively. The rupture of FRP sheets happens, noticing the maximum stress in FRP sheets exceeds the rupture stress.

It can be concluded that if good interfacial bond is guaranteed, increasing concrete fracture energy may result in different failure modes, from interfacial debonding to FRP rupture, and also affect the cracking behavior in concrete. Thus, the FRP strengthening effect is highly improved. Except the case of G_{Ic}=0.1N/mm, in which a diagonal crack pattern occurs, the other cases with secondary flexural crack or distributed crack seem

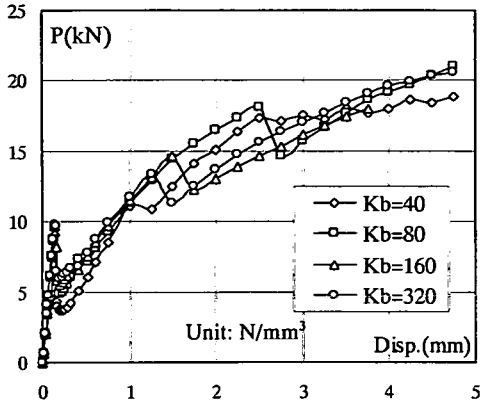

Fig. 26 Load-displacement curves with different K_b

to reach approximately the same load-carrying capacity.

(6) Initial Stiffness of Bond Interface K_b

Stiffness of bond interface used in present FE simulation is considered as a comprehensive property affected by surface concrete and adhesive layer. With different bond conditions and concrete Young's modulus, the value of K_b may be changed. In this section, the simulation results of four bond stiffness, with K_b=320, 160, 80 and 40N/mm^3, are compared. The other material properties are f_b=2.5MPa, G_{IIb}=1.2N/mm and G_{Ic}=0.1N/mm.

As seen in **Fig.26**, the bond stiffness does not affect much on load carrying capacity. But the cracking behavior in concrete is relatively influenced. The higher bond stiffness provides earlier stress transfer from FRP sheets to concrete so that the concrete stress level near mid span increases earlier. That is also why the diagonal crack occurs near the first flexural crack in higher bond stiffness K_b=320 and 160N/mm^3 while in case of K_b=80N/mm^3 the secondary flexural crack pattern happens a bit far away from the first one, as shown in **Fig.27**. If bond stiffness is too small, with K_b=40N/mm^3, the stress transfer cannot be well achieved. Therefore, cracks in concrete do not continuously propagate upward, and interfacial debonding failure occurs ultimately.

Since the concrete fracture energy is relatively low, all the 4 cases follow final interfacial debonding failure. Except the case of K_b=40N/mm^3

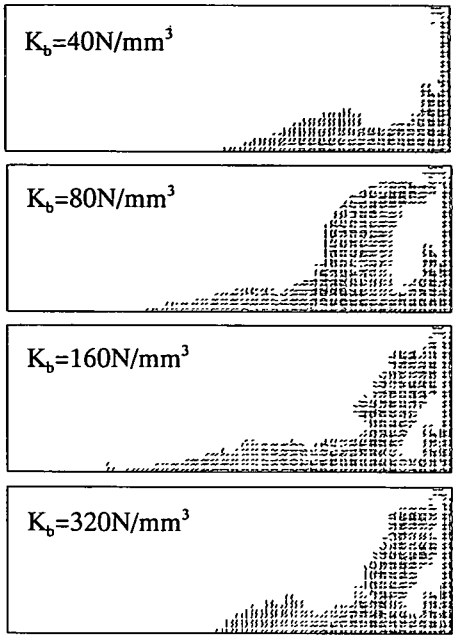

Fig. 27 Crack patterns with different K_b

whose crack pattern resembles the debonding type of **Fig.13**(b), the cracking behaviors of the other 3 cases with higher bond stiffness are considered to be similar to the debonding type as shown in **Fig.13**(c).

5. CONCLUSIONS

A comprehensive FE study on FRP-concrete interfacial bond behavior, concrete cracking behavior and strengthening effects of bonded FRP sheets in FRP-strengthened concrete beams is performed. Through a series of parametric numerical simulations and comparisons with the experimental results, the following conclusions could be obtained:

1) The ascending-descending bilinear τ–δ_t relation is considered to be simple and applicable to model the realistic interfacial bond and debonding behavior.
2) In the shear bond test, the load-carrying capacity of FRP-bonded concrete prism can be uniquely determined by the interfacial fracture energy G_{IIb}, Young's modulus and thickness of FRP sheets.
3) In FRP-strengthened concrete beams, the load

carrying capacity is quantitatively related to interfacial fracture energy G_{IIb} if concrete crack is localized with ultimate debonding failure that occurs in adhesive layer. But if distributed cracks occur, the load carrying capacity would also be influenced by other factors, such as concrete fracture energy G_{Ic}.

4) Local bond strength has effects on the peak load to some extent. But the propagation of debonding is mainly related to the interfacial fracture energy and concrete fracture energy.
5) Under the condition of good interfacial bond, the increase of concrete fracture energy G_{Ic} intends to result in a secondary flexural crack or distributed cracks in FRP-strengthened beams, thus improving FRP strengthening performance.
6) Stiffness of bond interface does not affect much of load carrying capacity, but has influence on the concrete cracking behavior.
7) The interfacial debonding failures that happen both within the adhesive layer and in concrete along the bond interface are important fracturing behaviors in FRP-strengthened beams. It is determined by the bond condition of adhesive layer and the concrete brittleness.

REFERENCES

1) Taljsten, B.: Strengthening of concrete prisms using the plate-bonding technique, Int. J. of Fracture, Vol.82, pp.253-266,1996.
2) Yuan, H., Wu, Z.S. and Yoshizawa, H.: Therotical solution on interfacial stress transfer of externally bonded steel/composite laminates, J. of Struc. Mech. and Earthquake Eng., JSCE, 2001.4.
3) Wu, Z.S. and Niu, H.D.: Study on debonding failure load of RC beams strengthened with FRP sheets, Journal of Structural Engineering,Vol.46A, pp.1431-1441, March 2000.
4) Wu, Z.S. and Niu, H.D.: Shear transfer along FRP-concrete interface in flexural members, Journal of Material, Concrete Structures and Pavements, JSCE, Vol.49, No.662, pp.231-145, November 2000.
5) Nishida, H., Kamiharako, A., Shimomura, T. and Maruyama, K.: Bond mechanism between continuous fiber and concrete, Proceedings of JCI, Vol.21, No.3, pp.1507-1512, 1999 (in Japanese).
6) Chajes, M.J., Finch, Jr. W.W., Januszka, T. and Thomson, Jr. T.: Bond and force transfer of composite material plates bonded to concrete, ACI Structural Journal, Vol.93, No.2, pp.208-217, March-April 1996.
7) Yoshizawa, H., Wu, Z.S., Yuan, H. and Kanakubo, T.: Study on FRP-concrete interface bond performance, Journal of Material, Concrete Structures and Pavements, JSCE, Vol.49, No.662, pp.105-119, November 2000 (in Japanese).
8) Wu, Z.S., Yuan, H., Yoshizawa, H. and Kanakubo, T.: Experimental/analytical study on interfacial fracture energy and fracture propagation along FRP-concrete interface, ACI International Convention, Special Publication 201, pp.133-152, 2001.
9) Wu, Z.S., Matsuzaki, T. and Tanabe, K.: Experimental Study of Fracture Mechanism of FRP-Strengthened Concrete Beams, JCI Symposium on FRP Reinforced Concrete Structures, JCI, pp.119-126, 1998.5 (in Japanese).
10) Yin, J. and Wu, Z.S.: Interface crack propagation in FRP-strengthened concrete structures using nonlinear fracture mechanics, FRPRCS-4, pp.1035-1047, Baltimore, Oct. 31-Nov. 5, 1999.
11) Yin, J., Wu, Z.S. and Asakura, T.: FE analysis on cohesion debonding and cracking behavior of FRP-strengthened concrete beams by nonlinear fracture mechanics, ACI International Convention, Special Publication 201, pp.267-281, 2001.
12) Feenstra, P., Borst, R. and Rots, J.: Numerical study on crack dilatancy, I: models and stability analysis, Journal of Eng. Mech., ASCE, Vol.117, No.4, pp.733-753, 1991.

(Received March 29, 2001)

FRP シート接着補強を有する構造部材の界面破壊メカニズムに関する数値シミュレーション

呉　智深・殷　峻

FRP シートの接着により補強されたコンクリート構造物の界面剥離は FRP 補強効果に大きな影響を与え，補強構造の重要な破壊モードと考えられる．本研究では，まず FRP シート接着の単純せん断実験結果に対して，幾つかの界面局所せん断応力—相対変位の関係を用いて，有限要素数値シミュレーションを行った．理論解析結果や実験結果との比較を行い，剥離発生後の線形軟化を有する局所せん断応力—相対変位の関係の有効性と正確性を検証した．さらに，4 つのパラメーターである接着界面の局所せん断強度・破壊エネルギー・剛性とコンクリートの破壊エネルギーが補強されたコンクリート梁の破壊モードとひび割れ分散状況に及ぼす影響を検討し，各種破壊モードの究明を行った．